J. Fluid Mech. (2007), *vol.* 590, *pp.* 35–60.
doi:10.1017/S0022112007007677 Printed in the United Kingdom

Numerical verification of the similarity laws for the formation of laminar vortex rings

M. HETTEL, F. WETZEL, P. HABISREUTHER AND H. BOCKHORN

University of Karlsruhe, Engler-Bunte-Institute, Division of Combustion Technology, 76131 Karlsruhe, Engler-Bunte-Ring 1, Germany
matthias.hettel@vbt.uni-karlsruhe.de.

(Received 8 March 2006 and in revised form 21 December 2006)

From analytical investigations it is well known that the roll-up of an inviscid plane vortex sheet which separates at the edge of a body is a self-similar process which can be described by scaling laws. Unlike plane vortices, ring vortices have a curved rotational axis. For this special vortex type experimental investigations as well as calculations in the literature suggest that the scaling laws are only partially valid. The main goal of this work is to clarify how far these similarity or scaling laws are also valid for the formation of viscid laminar vortex rings. Therefore, the formation process of laminar vortex rings was investigated numerically using a CFD (computational-fluid-dynamics) code. The calculations refer to an experimental setup for which detailed experimental data are available in the literature. In this setup, laminar ring vortices are generated by ejecting water from a circular tube into a quiescent environment by means of a piston. First, a case based on a constant piston velocity was investigated. Comparing calculated and measured data yields a very good agreement. Further calculations were made when forcing the velocity of the piston by three different time-dependent functions. The results of these calculations show that the formation laws for inviscid plane vortices are also valid for the formation process of viscid ring vortices. This applies to the normalized axial and radial position of the vortex centre as well as the normalized diameter of the vortex spiral. However, the similarity laws are valid only if the process is considered in a special frame of reference which moves in conjunction with the front of the jet and if the starting time of the formation process with respect to the starting time of the ejection is taken into account. Additionally, the formation of a ring vortex, which occurs during the start-up process of a free jet flow, was calculated. The results confirm a dependence for the motion of the jet front, which is known from analytical considerations and allows some interesting features to be identified.

1. Introduction

Vortices are ordered structures of fluid motion, which nature prefers over chaos in many situations (Lugt 1983). Therefore, vortex dynamics is a central theme within the research field of fluid dynamics. Vortices can be found in nature and technology and their length scale ranges from the fraction of a millimetre (turbulent eddies) to thousands of kilometres (planetary atmosphere). The formation of a vortex by roll-up of a vortex sheet, which separates at the edge of a body, is a phenomenon occurring in many flow configurations. Some examples are wing-tip vortices, vortices following

impulsively started flows around wedges and vortices formed by an amount of fluid pushed through an orifice.

Several authors have calculated the roll-up of an inviscid plane vortex sheet by applying different analytical methods. Kaden (1931) started his research from the flow around a semi-infinite plane discontinuity sheet. Continuative analytical calculations were done by Anton (1939) and Wedemeyer (1961). They theoretically studied the roll-up of a plane vortex sheet separating from the edge of a flat plate impulsively set into motion perpendicular to itself. Pullin (1978) calculated the roll-up of a semi-infinite vortex sheet and the vortex formation downstream of an infinite wedge. From these investigations it is well known that the evolution of roll-up of a plane inviscid vortex sheet is a self-similar process and obeys a typical time dependence of the form $\sim t^{2/3}$.

Unlike planar vortices, ring vortices have a curved rotational axis. They can occur both as free and as bounded vortices. An example of a bounded ring vortex is the vortex downstream of a sphere. In the case of small velocity the vortex does not detach. The energy which is needed to maintain the vortex flow is supplied by the external flow. In the case of a free ring vortex the kinetic energy is contained within the vortex and moves with it. Free or unbounded ring vortices can be created by ejecting an amount of fluid from a circular nozzle. During the vortex life cycle the fluid inside it exchanges with the ambient fluid. Most of the technical uses of ring vortices are based on the fact that ring vortices can transport fluid through a resting environment over long distances. Vortex rings have been studied for more than a century and numerous theoretical and experimental investigations have been conducted. An overview can be found in Lugt (1983), Shariff & Leonard (1992) and Saffman (1992). In the following we restrict our consideration to free laminar vortex rings.

Very detailed experimental data concerning free vortices have originated from the research group of the Max-Planck-Institut für Strömungsforschung in Germany. Vortex rings were created by ejecting fluid from a circular nozzle by means of a piston. Didden (1977, 1979), Liess & Didden (1976), Liess (1978) and Schneider (1978, 1980) examined all stages of the life cycle of free laminar vortex rings. More experimental investigations can be found for example in Maxworthy (1972, 1976), Durst & Fuchs (1974), Sallet & Widmayer (1974), Gühler & Sallet (1979), Glezer (1988), Southerland *et al.* (1991) and Fabris & Liepmann (1997).

For the numerical calculation of ring vortices there are mainly two basic approaches: solving the Navier–Stokes equations and vortex methods. Solving the Navier–Stokes equations implies the Eulerian frame of reference and applying numerical schemes like the finite-difference, finite-element or finite-volume method. These procedures demand substantial computational resources and very accurate numerical schemes to resolve the large gradients in the flow and mixture field of a vortex ring. One advantage is that the effect of viscosity is implied in the calculation. Results of ring-vortex calculations are discussed by James & Madnia (1996), Heeg & Riley (1997), Rosenfeld, Rambod & Gharib (1998) and Mohseni, Ran & Colonius (2001).

Vortex methods assume that an incompressible flow can be characterized by regions of concentrated vorticity, embedded in irrotational fluid. Within these regions, the inviscid motion of the vorticity is given by the local fluid velocity which in turn is determined kinematically from the vorticity field. Vortex methods simulate flows of this type by discretizing the vorticity-containing regions and tracking this discretization in a Lagrangian frame of reference. An overview on vortex methods is given in Leonard (1980). One benefit of such methods over the Eulerian schemes is that they require only a relative small number of storage locations. Disadvantages

concern the treatment of the no-slip condition at walls and of viscous effects. Results can be found in Chorin & Bernard (1973), Moore (1974), Seno, Kageyama & Ito (1988), Brady, Leonard & Pullin (1998), Nitsche & Krasny (1994) and Nitsche (1996, 2001).

Seemingly contradictory results have been obtained, both for the predictions and the measurements of motion and circulation of vortices generated at sharp edges. Therefore, various explanations have been given as to why the trajectories and circulations of ring vortices do not follow classical similarity-theory predictions. Didden (1979) argued that the rotational axis of a ring vortex, in contrast to a plane vortex, is curved. Subsequently, Auerbach (1987) performed an experimental study of two-dimensional vortex pair formation at the edge of a rectangular tube. He observed the same discrepancy between similarity theory and experiment as in the case of vortex rings. Nitsche *et al.* (1994) and Nitsche (1996) simulated the experiments performed by Didden. They developed an axisymmetric vortex sheet model for vortex ring formation at the edge of a circular tube. The comparison with the experimental data showed that the model accurately recovers the measured trajectories. Comparable results were obtained by James & Madnia (1996) and Heeg & Riley (1997) by solving numerically the Navier–Stokes equations.

The obvious difference between measurement and calculations on the one side and the analytical calculations on the other side lies in the time-dependence of the axial position X_V of the vortex ring. Both measurements and calculations resulted in $X_V \sim t^{3/2}$. However, the similarity laws for plane vortices predict $X_V \sim t^{2/3}$.

The main goal of this work is to investigate under which circumstances the formation process is self-similar and the origin of the difference to the similarity laws of inviscid plane vortices. In the work, the formation process of viscid laminar ring vortices was calculated numerically applying a CFD (computational-fluid-dynamics) code which uses the finite-volume method. First, the experiment performed by Didden (1979) was simulated. There, the vortices were produced by ejecting water from a pipe into a resting environment by means of a piston. After a short acceleration process, the piston reached a constant velocity. Additional CFD calculations using time-dependent piston velocities have been performed in order to investigate exclusively the formation process.

The motivation of the calculations was the investigation of the pulsating turbulent premixed jet flames which appear in connection with self-excited pressure oscillations in technical combustion systems. Depending on the amplitude and frequency of the pressure oscillations, large-scale turbulent ring vortices develop near the burner nozzle and interact with the reaction zone. More details concerning the calculation of pulsed laminar and turbulent jets and premixed turbulent jet flames, and the formation of laminar and turbulent vortex rings can be found in Hettel *et al.* (2004, 2005) and Hettel (2006).

2. Basics

2.1. *Formation of vortex rings*

2.1.1. *Ring vortices and their life cycle*

Ring vortices are vortex flows with a closed rotational axis which is circular. Figure 1 shows a schematic view of a fully formed, stable, laminar vortex ring of diameter D_V (Liess 1978). The toroidal form of the axis of the vortex core induces a

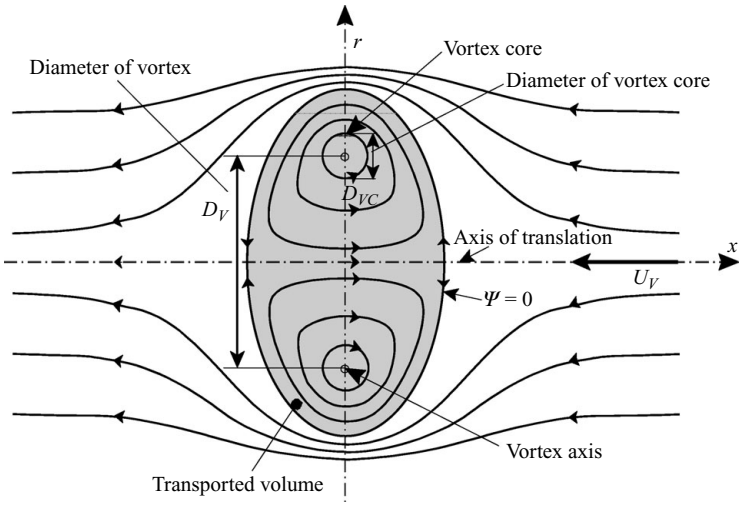

FIGURE 1. Schematic illustration of a stable laminar vortex ring in a vortex-fixed coordinate system (Liess 1978).

translational velocity U_V on itself. The vortex is shown in a frame of reference which moves together with the vortex. Therefore, the axial velocity far upstream of the vortex is U_V. Additionally some isolines of the stream function (equation (11) below) are shown. The streamline $\Psi = 0$ separates the vortex from the ambient fluid. The fluid within the grey region is circulated around the vortex core. During the vortex life cycle, there is little exchange between the fluid inside the vortex core, a region with a typical diameter $D_{VC} \approx 0,04 D_V$ (Liess 1978), and the ambient fluid, while there is a non-negligible exchange of ambient fluid with the vortex fluid outside the core. Thus, a ring vortex can transport the fluid inside the core region over long distances. In the literature many examples can be found where ring vortices were examined for their ability to transport gaseous fluids over long distances (i.e. exhaust gases, cooling air, narcotics).

The life cycle of free ring vortices can be divided into the following stages (Liess 1978):

1. vortex formation;
2. separation from the orifice;
3. stable laminar stage;
4. wavy stage;
5. transition stage;
6. turbulent stage;
7. phase of disintegration.

Figure 2 shows a comparison of the calculation and measurement of the trajectory (radial position versus axial position) of the vortex centre for the first three stages. Additionally, a calculated mixture field is shown for every phase. The boundary conditions can be found in § 3. During the formation process, the diameter of the vortex ring increases until the flow ceases. Subsequently, there is an abrupt contraction of the ring due to the influence of the nozzle boundary and due to the formation of a secondary vortex ring which occurs when the piston stops and which moves upstream into the nozzle (Didden 1979).

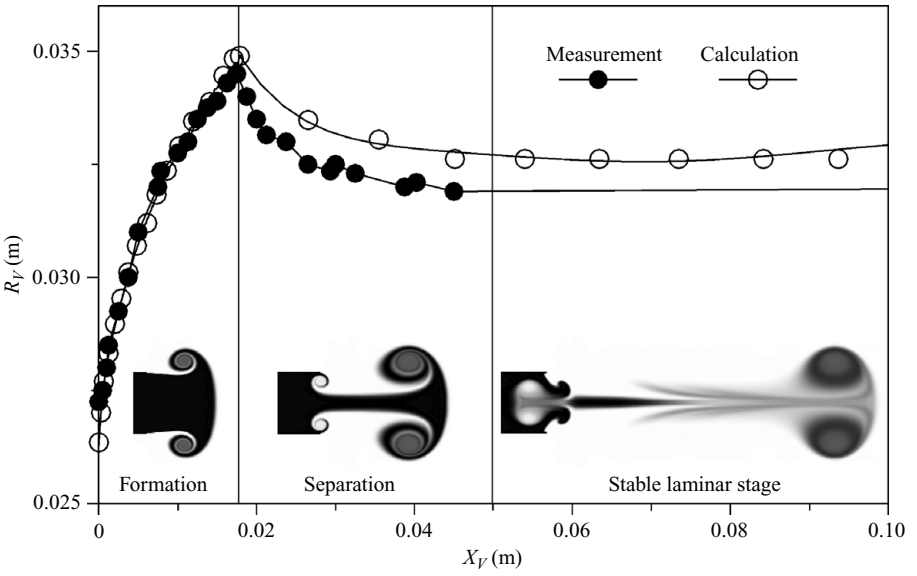

FIGURE 2. Comparison between calculated and measured (Didden 1979) vortex trajectory.

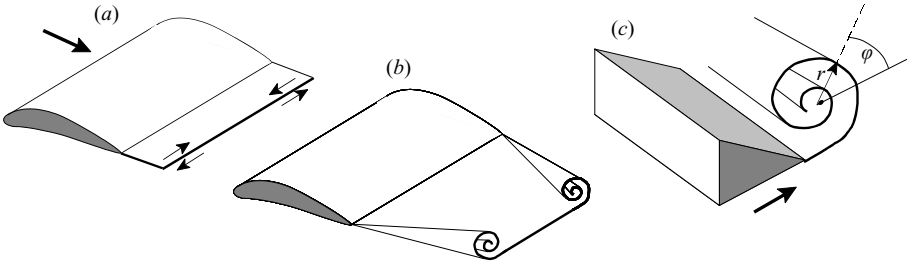

FIGURE 3. (a, b) roll-up of a discontinuity sheet at a wing tip (see Kaden (1931)); (c) roll-up of a discontinuity sheet at a sharp edge (see Prandtl 1924).

During the separation from the orifice, the vortex reaches the stable laminar stage. In this stage the translational velocity U_V decreases nearly linearly and the axial position of the centre and the diameter scale with $X_V \sim \log(t)$ and $D_V \sim t^k$, respectively, where k is dependent on the formation conditions (Liess 1978). The result of the calculation coincides with the measurement during the formation process. During the stage of separation the calculated radial positions are slightly larger than the measured data; the difference between the calculated and measured radius of the vortex ring is about 1 mm. The deviation is about 3%. In this paper only the process of vortex formation is discussed, while extensive calculations, on the phases of separation and the stable stage of laminar vortex rings, can be found in Hettel (2006).

2.1.2. *The roll-up of free discontinuity layers*

The investigation of the roll-up of a discontinuity layer is motivated by the theory of aircraft wings. Downstream of the trailing edge of a wing, a free shear layer occurs which rolls up at the wing tips (figure 3a, b). This is unwanted, because the induced drag of a wing with a given lift is minimal if no roll-up occurs. Furthermore, the separated layer influences the flow of the elevator unit of an aircraft. The same

phenomenon occurs in all technical applications where similar body shapes are used (i.e. turbo machinery).

Prandtl (1924) was the first to state, that the roll-up of a planar discontinuity sheet which appears in the flow around a sharp edge of a body is a self-similar process. He supposed that the structure of the spiral follows a logarithmic law $r = \text{const.}/\varphi^n$ (r and φ are polar coordinates and n is a number) (figure 3*c*). He also stated that the form of the underlying similarity laws should exhibit the characteristics of a power law.

2.1.3. *Self-similarity of the formation of vortex structures*

Kaden (1931) investigated the roll-up of ring vortices downstream of a wing (figure 3*a*, *b*) with detailed analytical calculations. The starting point was the flow around a semi-infinite inviscid plane discontinuity sheet (see figure 17*a* below). This flow can be obtained using the conformal transformation of a flow along a plane wall. As a result, Kaden (1931) showed that the velocities at positions which are located in a polar coordinate system at a constant angle φ ('similar' positions) are proportional to $1/\sqrt{r}$. As the flow directions are constant the 'similarity' exists in the whole flow region. Kaden (1931) made the following considerations: Take two distinct regions of the flow field, where one region is n times larger than the other region. Then take two points, each in one of the regions at the same relative ('similar') position and observe the changes that occur. As the starting velocities at the two points are proportional to each other, the movements of the two points are also proportional to each other. The changes of the shape of the streamlines in each region are similar. But the duration of the same process will be larger in the bigger region than in the smaller region. This is because the velocities in the bigger region are smaller by the factor $1/\sqrt{n}$ and the distances covered are greater by the factor n. The time needed to obtain similar changes inside the big region as in the small region therefore is larger by the factor $n\sqrt{n} = n^{3/2}$. As a result, a flow pattern which exists at the time t_1 of the process in the small region occurs at time $t_2 = n^{3/2} t_1$ in the region which is n-times larger. Thus, the times t_1 and t_2 of the similar flow patterns are related to the length scales r_1 and r_2 as follows:

$$\frac{t_2}{t_1} = n^{3/2} = \left(\frac{r_2}{r_1}\right)^{3/2} \quad \text{or} \quad \frac{r_2}{r_1} = \left(\frac{t_2}{t_1}\right)^{2/3}. \tag{1}$$

Subsequently Kaden (1931) analytically calculated the time-dependent shape of the vortex spiral. A comparison with experiments verified the findings. Follow up analytical calculations were done by Anton (1939) and Wedemeyer (1961). They theoretically studied the roll-up of a plane vortex sheet, separating from the edge of a flat plate impulsively set into motion perpendicular to itself. An overview of the similarity laws for different types of geometries can be found in Saffman (1978). There, the similarity laws are given in dimensionless form:

$$X^* \sim (t^*)^{2/3}, \quad Y^* \sim (t^*)^{2/3}, \quad D_s^* \sim (t^*)^{2/3}. \tag{2}$$

X^* is the normalized axial distance of the vortex centre and Y^* the normalized radial distance relative to the nozzle edge. D_S^* is the diameter of the inner vortex spiral. All values are normalized as follows, where U_{char} is a characteristic velocity and L_{char} a characteristic length scale

$$X^* = \frac{X}{L_{char}}, \quad Y^* = \frac{Y}{L_{char}}, \quad D_s^* = \frac{D_s}{L_{char}}, \quad t^* = t\frac{U_{char}}{L_{char}}. \tag{3}$$

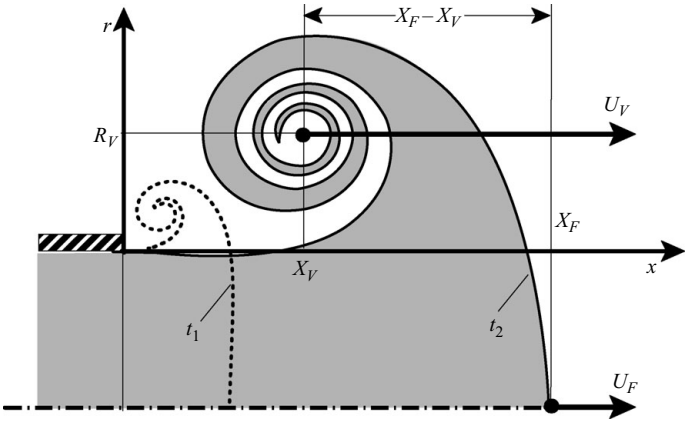

FIGURE 4. Schematic illustration of the formation process.

In non-normalized form the relations given in (2) can be written as

$$X = C_1\,(\alpha t)^{2/3}, \quad Y = C_2(\alpha t)^{2/3}, \quad D_s = 2\big(C_4^2/C_3^2\big)(\alpha t)^{2/3}, \tag{4}$$

C_1, C_2, C_3 and C_4 are constants; α depends on the geometry of the problem and on the flow far from the formation region. First, the scaling laws are developed for planar vortices considered to be infinitively long and showing no curvature of the rotational axis (two-dimensional vortices). These scaling laws are only valid as long as the dimension D_S of the vortex spiral is much smaller than the characteristic length scale L_{char} (i.e. nozzle diameter, channel height, length of plate) of the appropriate geometry.

2.1.4. *Start-up procedure of a laminar free jet flow*

Another interesting phenomenon is the formation of a ring vortex which occurs during the start-up procedure of a laminar free jet flow. If a nozzle flow is started and is held constant over time, a steady-state laminar free jet flow will arise after an infinitely long time span. At the beginning of the start-up procedure a vortex ring occurs at the nozzle edge and moves downstream together with the front of the jet. Figure 4 shows the shape of the fluid emanating from the nozzle for two different times $t_1 < t_2$. The intersection of the line which separates nozzle fluid from ambient fluid with the symmetry axis is called the 'front position' X_F of the jet. This definition is also valid for the formation process of an isolated vortex ring and will be used to discuss the similarity laws.

Referring to Prandtl (1924) (cited by Wille 1952) the velocity U_F of the front can be determined easily. First, the process is examined in a fixed frame of reference (figure 5*a*). The front position X_F moves with the velocity U_F in the positive x-direction. Thus, the velocity of the jet coming from the left is U_{nozzle}. In figure 5*b* the process is shown in a coordinate system which moves with the jet front. Now, the front position is fixed at the stagnation point. The velocity of the jet flowing from the left is then $U_{nozzle} - U_F$. On the basis of the law of Bernoulli, we find that at the stagnation point the relation

$$(U_{nozzle} - U_F)^2 = U_F^2 \tag{5}$$

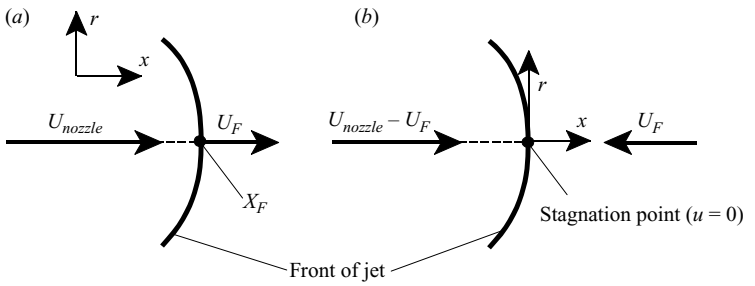

FIGURE 5. Conditions at the jet front; (*a*) fixed coordinate system; (*b*) moving coordinate system.

is valid, leading to

$$\frac{U_F}{U_{nozzle}} = 0.5. \tag{6}$$

The ratio of front and jet velocities becomes 0.5. Wille (1952) performed experimental investigations and found ratios from 0.55 to 0.8, depending on the Reynolds number. However, the measurements of the flow velocity were not very exact. The relation given in (6) was confirmed by Liess (1978). He showed that the translational velocity of a single ring vortex increases with the volume of fluid ejected. The longer the ejection time is, the closer the translational velocity converges towards an asymptote given by half of the nozzle exit velocity. Therefore, a continuous changeover of the translational velocity exists from a single isolated vortex to a vortex which is bounded at a jet front.

2.2. *Numerics*

2.2.1. *The CFD code CATS-2D*

For the calculations we applied the CFD (computational fluid dynamics) code CATS-2D (Combustion and Turbulence Simulator 2-dimensional). This code was developed at the Engler-Bunte-Institute based on the TEACH-code (Gosman & Ideriah 1976) and uses the finite-volume method. In it, the Navier–Stokes equations in axisymmetrical form are numerically solved on a staggered two-dimensional grid using a primitive variable formulation. For pressure–velocity coupling the CFD code uses the SIMPLEC algorithm and the Tri-Diagonal-Matrix-Algorithm for solving. The details of the numerical model are standard (Patankar 1980). For discretization of the convective terms of the transport equations the bounded high-resolution MLU (Monotonized Linear Upwind) scheme by Noll (1992) was implemented. It exhibits second-order accuracy. The temporal discretization is handled by an implicit first-order time-stepping.

For the analysis of the convergence of a CFD calculation it is usual to sum the residual of each cell and to normalize the sum with a global value, i.e. the mass flow entering the calculation domain. This procedure is not helpful if the mass flow changes in time or is zero (in our case after the piston has stopped). Therefore we used a different criterion for the convergence analysis (Hirsch 1995). The starting point is the general form of the transport equation (Patankar 1980):

$$\frac{\partial(\varrho\Phi)}{\partial t} + \nabla(\varrho \boldsymbol{u}\Phi) - \nabla(\Gamma\nabla\Phi) = S_\Phi, \tag{7}$$

where Φ is the transported quantity, Γ the diffusion coefficient and S_Φ the source term. The discretized equation for the cell P for fully implicit time discretization (new = new time step, old = old time step) is (Patankar 1980)

$$a_P(\Phi_P)^{new} = \sum_{nb} a_{ab}(\Phi_{nb})^{new} + S_{\Phi,P} \tag{8}$$

with

$$a_P = \sum_{nb} a_{nb} + \frac{\varrho_P^{old}}{\Delta t} V_P - (S_{\Phi,P,lin.})^{new}, \quad S_{\Phi,P} = \left((S_{\Phi,P,const})^{new} + \frac{(\varrho\Phi)_P^{old}}{\Delta t} \right) V_P.$$

The coefficients a_{nb} contain the convection and diffusion fluxes of the cells in the neighbourhood of cell P with the volume V_P. $S_{\Phi,P,const.}$ is the constant part and $S_{\Phi,P,lin.}$ the linearized part of the source term S_Φ. The residual of equation (8) for cell P for a certain iteration k is

$$(Res_P)^k = \sum_{nb} a_{nb}(\Phi_{nb})^k - a_P(\Phi_P)^k + (S_{\Phi,P})^k. \tag{9}$$

A relative error for this equation can be calculated based on the consideration that the right-hand side equals zero for convergence. In this case the term with the largest absolute value is balanced with the sum of the other terms. This means that this term is characteristic for the equation and can be used to normalize the residual. An applicable average residual results from the summation of the individual terms over all cell volumes:

$$Res = \frac{\sum_i |(Res_i)^k|}{\sum_i (\max(|\sum_{nb} a_{nb}(\Phi_{nb})^k|, |a_P(\Phi_i)^k|, |(S_{\Phi,i})^k|))} \leqslant 10^{-5}. \tag{10}$$

At the beginning of the calculations the residual *Res* has typical values of order of magnitude of 1. The convergence criterion was set to 10^{-5} (§ 2.2.2). This relates directly to the calculation accuracy of a computer working with real numbers on a 4-byte description, which is about six decades for the addition.

2.2.2. *Analysis of computational accuracy*

To analyse the quality of the numerical solution, the influence of grid size, time step and residual limit on the results was investigated. Figure 6 shows the trajectory of the vortex centre during the formation stage (see figure 2) using different numerical parameters. The boundary conditions can be found in § 3.

Part (*a*) of figure 6 shows the influence of the grid size for a fixed time step and residual limit. The results using the grids of 150×90 and 300×180 nodes coincide. The grid with 75×45 nodes shows a deviation of the calculated values. Additionally, the values are not as smooth as for the two finer grids. The algorithm for searching for the position of the vortex centre indicates in which cell it is to be found (see § 3.1.3). However, the exact position within a finite volume remains unknown. Therefore, the cell index and the appropriate position remains constant during some time steps and then jumps to the next cell. The result using the coarsest grid is still reasonably satisfactory. The grid lines in the formation region of the vortex are denser than in the far region. Obviously the density in the formation region is sufficient to yield an approximate solution even for the coarsest grid.

The influence of the time step for the 300×180 grid is shown in part (*b*) of figure 6. For a time step of $\Delta t = 0.001$s and smaller the results coincide. A time step of $\Delta t = 0.035$s leads to a deviation of the results towards larger radial values.

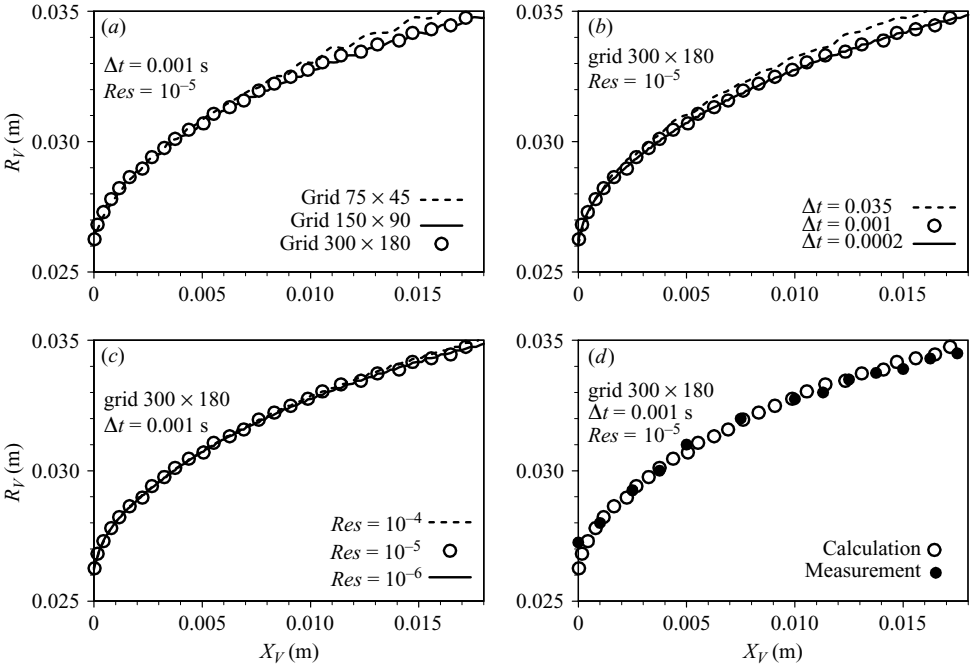

FIGURE 6. Influence of numerical parameters on the trajectory of the vortex centre: (*a*) grid size, (*b*) time step, (*c*) residual limit, (*d*) calculation versus measurement.

Part (*c*) of figure 6 shows the influence of the residual limit for the grid with 300×180 cells. For $Res = 10^{-5}$ and smaller the results coincide. A very small deviation can be found for a residual limit of $Res = 10^{-4}$. This result demonstrates, that the formulation of the residual described in § 2.2.1 ensures an accurate solution even for values of the limit of the order of 10^{-4}.

The results show, that using a grid with 300×180 cells, a time step of $\Delta t = 0.001$ s and a residual limit of $Res = 10^{-5}$ guarantees solutions which are independent of these numerical parameters. We used these values of the parameters to obtain all the results shown below. A comparison between the calculation and the measurement of Didden (1979) is shown in part (*d*) of figure 6. The correspondence between calculation and measurement is nearly perfect.

3. Calculation of laminar vortex rings

3.1. *Approach*

3.1.1. *Investigated system*

The system used to calculate the vortex formation, was the same as used by Didden (1979) for his experimental investigations (figure 7). It consists of a circular tube immersed in a water-filled tank. The separated flow is produced by ejecting water from the tube into the quiescent environment by means of a piston. After a short acceleration process, the piston reaches a constant velocity. $L_{piston}(t)$ denotes the time-dependent position of the piston. Due to the viscosity of the fluid, a boundary layer grows at the inner wall of the pipe. The boundary layer separates at the nozzle edge, rolls up and forms a vortex ring. The circulation of the vortex ring originates from

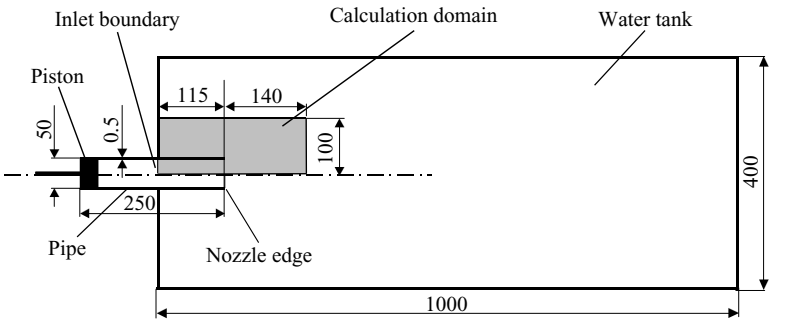

FIGURE 7. Geometry of the experimental system and definition of the calculation domain, dimensions in mm.

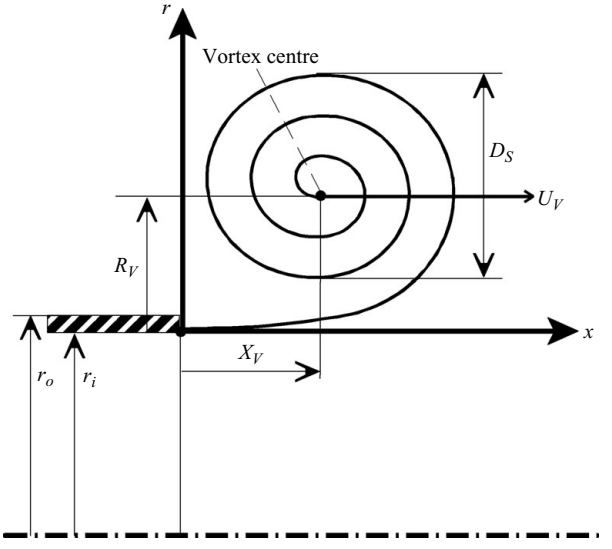

FIGURE 8. A schematic view of the vortex spiral. X_V and R_V are the coordinates of the vortex centre. D_s is the diameter of the vortex spiral and U_V is the translational velocity of the vortex. The origin of the cylindrical coordinate system is located at the inner nozzle edge.

the detached boundary layer. After the formation stage, the vortex separates from the nozzle and reaches the stable laminar stage.

The grey region in figure 7 represents the size and the position of the calculation domain. For all results shown below, we used the grid with 300×180 cells in the axial and radial directions, respectively (see § 2.2.2). On the symmetry axis of the domain, symmetric boundary conditions were used. All other boundaries were defined as open boundaries, where inflow or outflow is possible. To simulate the motion of the piston, the axial velocity at the inlet boundary of the calculation domain was set equal to the piston velocity by means of a plug-flow profile.

Figure 8 shows a schematic view of the ring vortex, the coordinates of the vortex centre (X_V, R_V), the diameter of the vortex spiral D_S and the direction of the translational velocity U_V. The origin of the cylindrical coordinate system is located at the inner nozzle edge.

The following properties for the water were used: $\varrho = 1000\,\mathrm{kg\,m^{-3}}$, $\nu = 10^{-3}\ \mathrm{m^2\ s^{-1}}$. To distinguish between the fluid emanating from the nozzle and the ambient fluid,

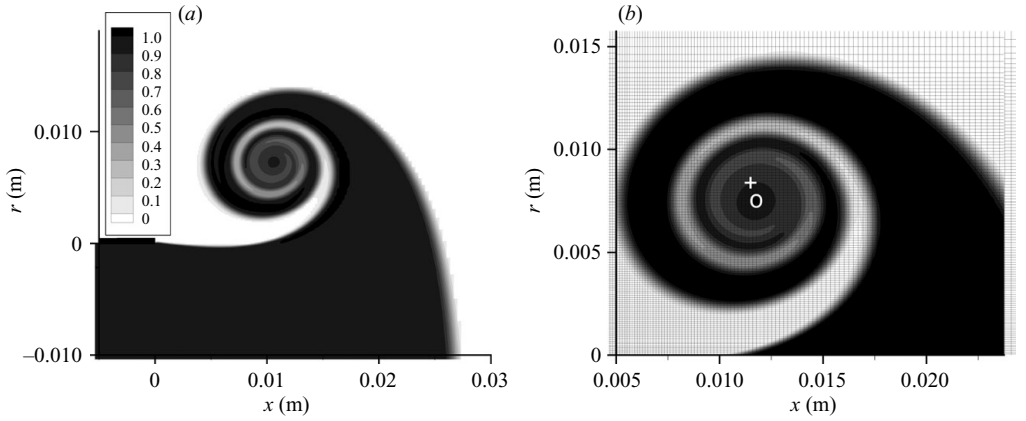

FIGURE 9. Normalised concentration of scalar f; (b) is an enlargment of (a).

an additional transport equation for the scalar quantity f was solved. The molecular diffusion coefficient $\Gamma_{diff} = \nu/Sc$ of the additional transport equation was determined with a Schmidt number of $Sc = 400$.

3.1.2. *The diameter of the vortex spiral*

In the experiments by Didden (1979) the vortex was visualized by injecting dye into the pipe through a narrow slot near the nozzle edge. Photos of the dyed vortex rings show a distinct structure which could be analysed to derive the spiral diameter. In the calculation a different approach was used. At the beginning of the calculation the value of the additional scalar f was set to unity in the region of the flow inside the tube. The diameter of the vortex spiral was obtained by analysing the mixture field of the scalar f (figure 9a).

Thereby, the maximal and minimal radius of the vortex spiral at the axial position of the vortex centre X_V was identified. Thus, the diameter of the vortex spiral D_S is determined by the difference between these two radial positions (see figure 8). To obtain an impression of the spatial resolution, figure 9(b) shows an enlargement of a section of 9(a) together with the computational grid (300×180 cells).

3.1.3. *Detection of the vortex centre*

The vortex centre was identified by detecting the maximum of the stream function. Therefore, an algorithm was implemented in the CFD code, which analyses the distribution of the stream function Ψ and the spatial position of its maximum for each time step. For an axisymmetrical flow the stream function is defined as follows:

$$\Psi(x, r) = 2\pi \int_0^r u(x, r) r \, \mathrm{d}r - 2\pi r \int_0^x v(x, r) \, \mathrm{d}x. \tag{11}$$

The position of the maximum of the stream function for the time step shown in figure 9(b) is marked by a white cross.

A second characteristic of vortices can be extracted from the Navier–Stokes equations transformed into a cylindrical coordinate system. For a steady-state plane vortex the Navier–Stokes equation in the radial direction yields

$$\frac{w^2}{r} = \frac{1}{\varrho} \frac{\partial p}{\partial r}. \tag{12}$$

The gradient of static pressure is positive in the whole flow region. Towards the rotational axis the pressure decreases, reaching its minimum at the vortex centre. The position of the minimum of the static pressure for the time step shown in figure 9(*b*) is marked by a white circle. For ring vortices, which have a small translational velocity U_V, the positions of the maximum of the stream function and the minimum of the static pressure nearly coincide. With regard to the analysis here, it was insignificant which of the two positions was used. But the faster a ring vortex moves in the axial direction the more the two positions differ. This should be kept in mind, especially while analysing turbulent vortex rings (Hettel *et al.* 2004, 2005; Hettel 2006).

3.1.4. *Calculation of circulation*

The change of circulation $\mathrm{d}\Gamma$ within the region $x > 0$ during the time interval $\mathrm{d}t$ is given by $\mathrm{d}\Gamma = \int_A \omega \,\mathrm{d}A$, where $\omega = (\partial v/\partial x - \partial u/\partial r)$ is the vorticity. The integration region A in the (x, r)-plane contains all the fluid that convects through the plane $x = 0$ during the interval $\mathrm{d}t$ (Didden 1979). Thus, the total circulation shedding rate is

$$\frac{\mathrm{d}\Gamma_t}{\mathrm{d}t} = \int_0^\infty \omega(x = 0, r, t) u(x = 0, r, t)\,\mathrm{d}r. \tag{13}$$

The total shedding rate is the sum of the circulation shed inside and outside the tube:

$$\frac{\mathrm{d}\Gamma_\mathrm{t}}{\mathrm{d}t} = \frac{\mathrm{d}\Gamma_i}{\mathrm{d}t} + \frac{\mathrm{d}\Gamma_o}{\mathrm{d}t} = \int_0^{r_i} \omega u \,\mathrm{d}r + \int_{r_o}^\infty \omega u \,\mathrm{d}r, \tag{14}$$

where r_i and r_o are the inner and the outer radii of the nozzle, respectively. The shed circulation is obtained from time integration of the shedding rates:

$$\Gamma_t = \Gamma_i + \Gamma_o = \int_0^t \frac{\mathrm{d}\Gamma_i}{\mathrm{d}t}\,\mathrm{d}t + \int_0^t \frac{\mathrm{d}\Gamma_o}{\mathrm{d}t}\,\mathrm{d}t. \tag{15}$$

3.2. *Results and discussion*

3.2.1. *Calculations with a time-limited constant velocity*

In this section results of the calculation referring to an experiment performed by Didden (1979) are discussed. The measured time-dependent position $L_{piston}(t)$ of the piston was fitted and used in the calculations as the boundary value of the axial velocity at the inlet boundary ($x = -0.115$ m) of the calculation domain (figure 7). After an acceleration phase of 0.3 s the piston velocity remains constant at $U_{piston} = 0.046\,\mathrm{m\,s^{-1}}$. Overall, the piston moves a dimensionless distance of $L_{piston,max}/D_{nozzle} = 1.4$.

The coordinates of the vortex centre ($X_V(t)$, $R_V(t)$) and the diameter of the vortex spiral $D_S(t)$ are normalized by the nozzle diameter $D_{nozzle} = 0.05$ m. The normalized time axis is defined using the position of the piston and the nozzle diameter. Although defined by two distances, it can be considered as a 'normalized time' (see § 3.2.2). Thus

$$X_V^*(t) = \frac{X_V(t)}{D_{nozzle}}, \quad R_V^*(t) = \frac{R_V(t)}{D_{nozzle}}, \quad D_S^*(t) = \frac{D_S(t)}{D_{nozzle}}, \quad t^* = \frac{L_{piston}(t)}{D_{nozzle}}. \tag{16}$$

Both abscissa and ordinate are shown in logarithmic scales to allow a comparison with the power laws of the similarity relations.

Axial velocity at the nozzle outlet plane

Figure 10 shows radial slices of the axial velocity at the nozzle tube outlet plane ($x = 0$ m) for different times ($t = 0.1$, 0.3, 1.6 s) after the beginning of the piston movement. The wall thickness of the nozzle tube is 0.5 mm. The inner edge of

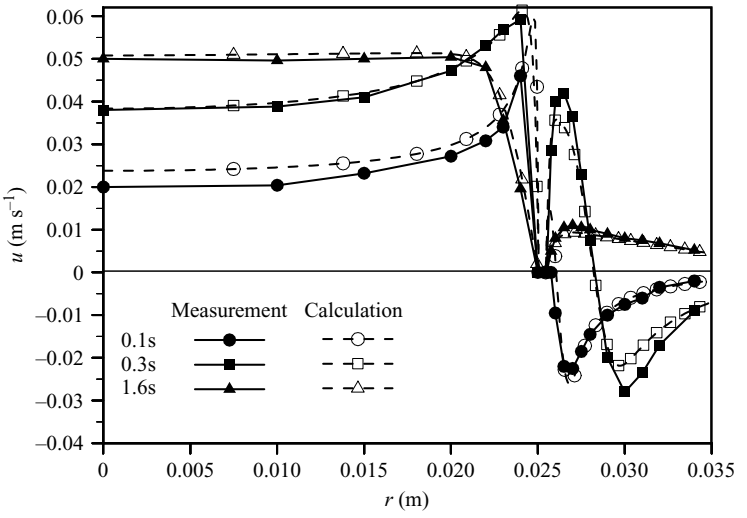

FIGURE 10. Comparison of measured and calculated axial velocity at the nozzle outlet plane.

the nozzle tube is positioned at $r_i = 0.025\,\mathrm{m}$, the outer edge at $r_o = 0.0255\,\mathrm{m}$. The calculated and measured velocities correspond very well for each time point. At the beginning of the ejection, a flow around the nozzle edge develops. Near to the inner wall, the fluid moves faster than at the symmetry axis. At the time of 0.3 s, the velocity near the inner wall is larger than the piston velocity of $U_{piston} = 0.046\,\mathrm{m\,s^{-1}}$. Downstream of the nozzle edge, the fluid moves radially outwards which leads to a backflow near to the outer wall of the tube. This behaviour corresponds to the beginning of vortex formation. As time proceeds the axial velocity near the inner wall decreases where the velocity in the interior region increases. The velocity profile reorganites towards the steady-state hyperbolical distribution, but this process has not finished at the maximum time calculated. As the vortex moves away from the nozzle edge, the backflow outside the nozzle vanishes and a boundary layer arises at the outer wall of the tube.

The calculated velocity profiles match better with the measurements than the results from the finite-difference calculations of Heeg & Riley (1997). However, the velocity profiles computed from Nitsche & Krasny (1994) differ considerably from the measurements. The vortex-blob model used is not able to satisfy the no-slip condition at the tube wall.

Axial position of the vortex centre

Figure 11 shows the normalized axial position of the vortex centre X_V^* versus the normalized time t^*. The result of the calculation coincides with the result obtained by the measurement. Both curves show a dependence which is proportional to $X_V^* \sim (t^*)^{3/2}$. Nitsche & Krasny (1994), James & Madnia (1996) and Heeg & Riley (1997) found the same characteristics in their calculations. But this behaviour contradicts the similarity law, which predicts a dependence proportional to $X_V^* \sim (t^*)^{2/3}$. The discussion of this finding in § 3.2.2 will show that this discrepancy can be explained by the fact that in each system (vortex formation behind a circular nozzle and roll-up of a semi-infinite free vortex sheet) a different frame of reference is used.

Radial position of the vortex centre

Figure 12 shows the normalized radial position of the vortex centre R_V^* versus normalized time t^*. The results of the calculation coincides with the result obtained

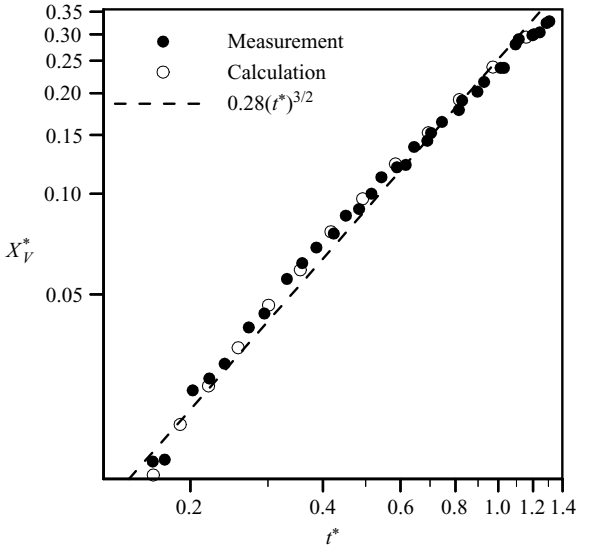

FIGURE 11. Normalized axial position of vortex centre versus normalized time.

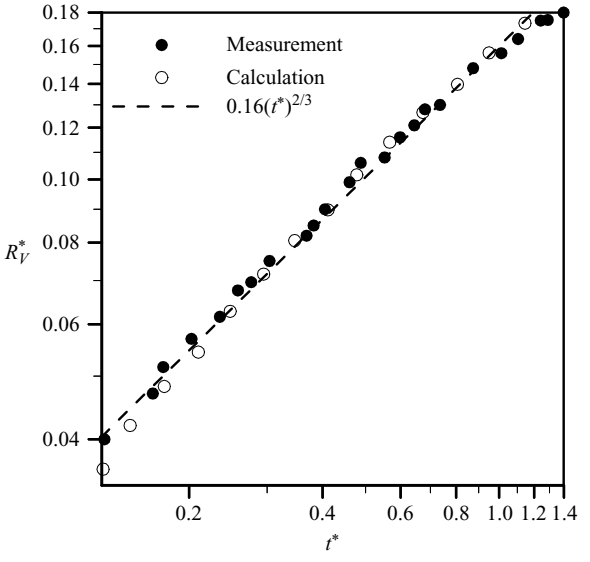

FIGURE 12. Normalized radial position of vortex centre versus normalized time.

by the measurements. The dependence of the radial position predicted by the similarity law $R_V^* \sim (t^*)^{2/3}$ can be reproduced by both calculation and experiment. Nitsche & Krasny (1994), James & Madnia (1996) and Heeg & Riley (1997) found the same characteristics in their calculations.

Diameter of the vortex spiral

Figure 13 shows the normalized diameter of the vortex spiral D_S^* versus normalized time t^*. The result of the calculation confirms the similarity law, which predicts the dependence $D_S^* \sim (t^*)^{2/3}$. But this result contradicts the result of the measurements, where the dependence $D_S^* \sim (t^*)^1$ was found. Possibly, this discrepancy between the result obtained by Didden (1979) and the similarity law is due to different definitions of

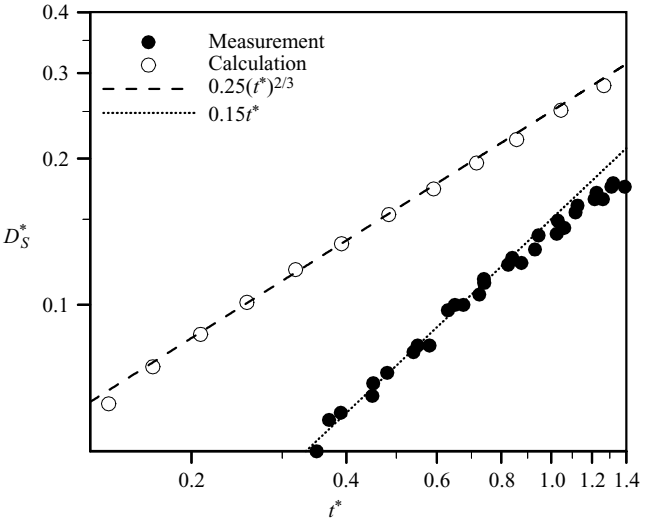

FIGURE 13. Normalized diameter of the vortex spiral versus normalized time.

the diameter of the vortex spiral. The diameter used by Anton (1939) and Wedemeyer (1961) for the analytical derivation of the similarity laws is clearly defined. It is the diameter of the region of the vortex where the convolutions of the spiral are approximately circular. This virtual diameter is an idealized approximation, needed for the solution of the analytical problem. The definition of the diameter of the vortex spiral used in this work can be found in figure 8. Clearly, the results using this definition are the same as the results predicted by the similarity law. The definition of the spiral diameter used by Didden (1979) remains questionable. However, there is a second reason to doubt the diameter measured by Didden (1979). As explained above, the formation process of the ring vortex is self-similar. This similarity is not only valid for the vortex centre, but also for all radial positions. As a consequence, the similarity law is also valid for the radial distance between two 'similar' radial positions and therefore also for the spiral diameter.

Circulation

Figure 14 shows a comparison of calculated and measured circulation which is convected through the plane $x = 0$. The positive circulation Γ_i shed from the inner wall and the negative circulation Γ_o shed from the outer wall of the tube both increase with time. As the vorticity flux decreases with time, the growth of the vorticity reduces (Didden 1979). If all vortical fluid that has been transported into the region $x > 0$ at the end of the stroke is rolled up into the vortex and if dissipation is neglected, the total circulation of the ring vortex is $\Gamma_t(t = 1.6\,\mathrm{s}) = \Gamma_i + \Gamma_o$ (see equation (15)). The total circulation Γ_t is considerably diminished by the flux of negative vorticity Γ_o which is produced at the boundary layer at the outer wall of the tube. Although the calculation predicts the characteristics of the measurements very well, the total amount of the inner and outer circulation is underestimated in each case. In contrast Heeg & Riley (1997) and Nitsche & Krasny (1994) both found an overestimation of the calculation versus the measurement. James & Riley (1996) got a better agreement, but, their results are normalized with the values at the end of the piston stroke.

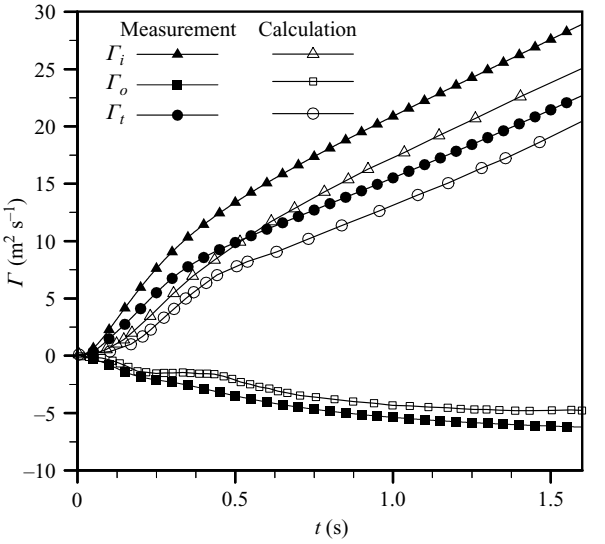

FIGURE 14. Calculated and measured circulation versus time.

3.2.2. *Calculations with time-dependent velocities*

In this section the influence of the piston movement on vortex formation was investigated using three different time-dependent functions for the velocity of the piston:

$$\left.\begin{aligned} &\text{linear function: } U_{piston}(t) = \bar{U}_{piston}\frac{2t}{t_{\max}},\\ &\text{sine function: } U_{piston}(t) = \bar{U}_{piston}\left(1+\sin\left[2\pi\frac{t}{t_{max}}-\frac{\pi}{2}\right]\right),\\ &\text{power function: } U_{piston}(t) = \bar{U}_{piston}\frac{1}{0.78568}t^{2.6}. \end{aligned}\right\} \tag{17}$$

As before, the velocity of the piston was used as the velocity of the fluid at the inlet boundary (figure 7). The time-averaged velocity $\bar{U}_{piston} = 0.046\,\mathrm{m\,s^{-1}}$ was the same as the constant velocity used in the calculations given in § 3.2.1. In figure 15(*a*) the time-dependent velocity $U_{piston}(t)$ is shown, and in part (*b*) the position of the piston $L_{piston}(t)$. Both quantities are plotted versus the physical time. The definitions of the velocity functions ensure that the ejected volume was the same in all cases. The maximum position of the piston was $L_{piston,max}/D_{nozzle} = 1.4$, and the maximum time of ejection was $t_{max} = L_{piston,max}/\bar{U}_{piston} = 1.522\,\mathrm{s}$ for all calculations.

Figure 15 (*c*) shows the total circulation shed. The time-dependent characteristics of the curves for the linear function and the power function are qualitatively the same. However, the curve of the sine function differs. For most of the ejection time, the circulation using the sine function is larger than for the other two functions. Only at the end of the ejection stroke is the total circulation using the power function largest. The translational velocity of a fully formed stable vortex is proportional to the circulation $U_V \sim \Gamma_V$ (Saffmann 1978). If all vortical fluid is accumulated in the vortex, it can be expected that the stable laminar vortex which is formed using the power function exhibits the largest translational velocity.

Figure 15 (*d*) shows the trajectories of the vortex centre during the formation process. Again, the curves for the linear and power functions are qualitatively

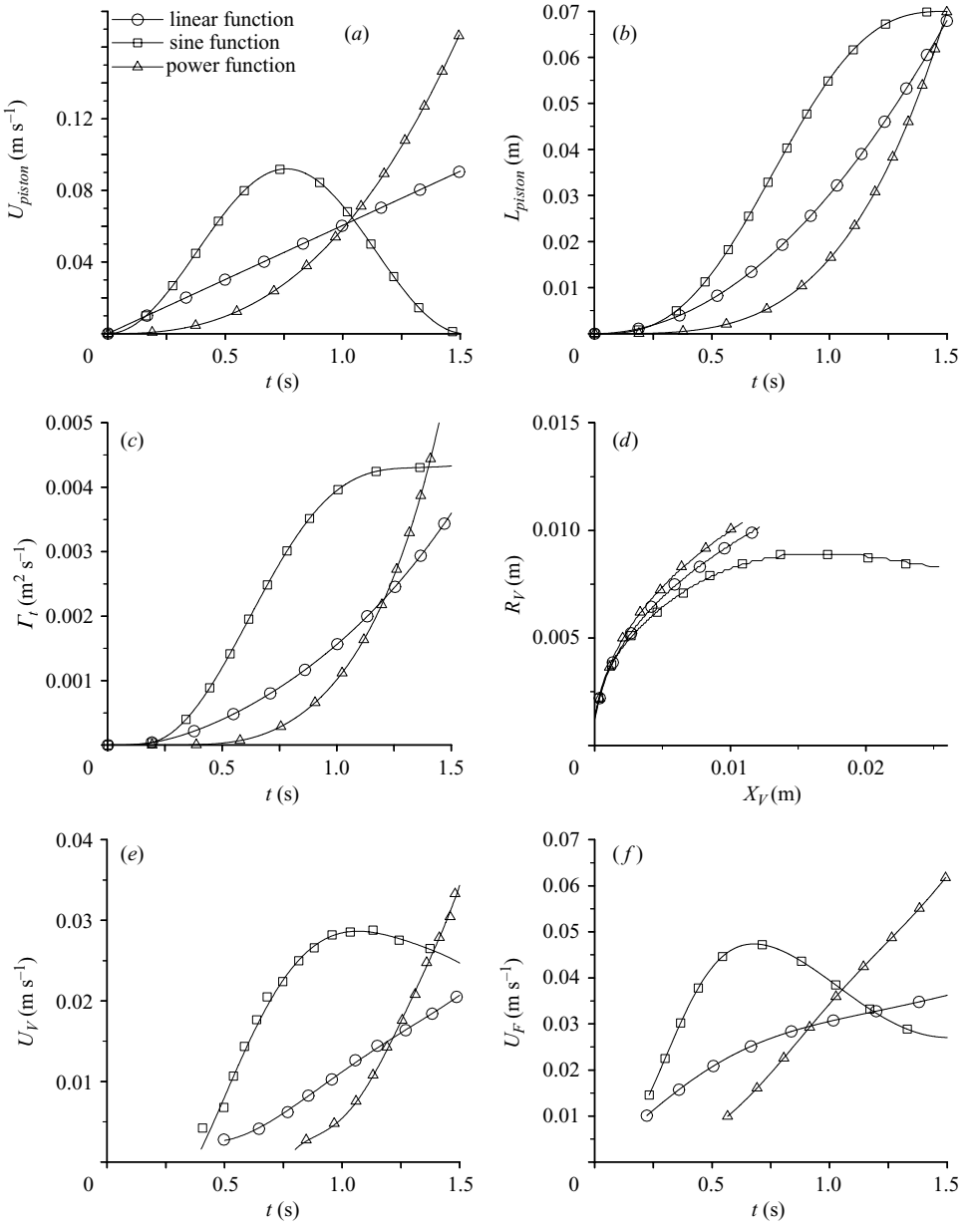

FIGURE 15. Calculations with variation of piston velocity function: (*a*) velocity of piston U_{piston}; (*b*) position of piston L_{piston}; (*c*) total circulation Γ_t; (*d*) vortex trajectory; (*e*) velocity of vortex centre U_V; (*f*) velocity of jet front U_F.

comparable. Surprisingly, the maximum axial position the vortex reaches for the sine function is nearly twice the maximal axial positions of the two other velocity functions. This behaviour can be deduced from figure 15(*e*) and (*f*), where the axial velocity of the vortex centre U_V and the axial velocity of the jet front U_F are shown. For both the linear function and the power function, the piston accelerates during the whole ejection time (see part *a*). Correspondingly both velocities U_V and U_F increase. The acceleration of the piston is largest for the sine function (see part *a*). It is the only

velocity function which exhibits a deceleration phase. At the end of the stroke, the piston velocity is zero. The respective velocities U_V and U_F both exhibit a deceleration phase which is shorter in time and smaller in magnitude than the acceleration phase. The momentum which is imparted to the fluid at the beginning of the formation process is only partly discharged at the end of the formation process. Therefore, the vortex moves over a larger axial distance using the sine function in contrast using the other two velocity functions (see part *d*). James & Madnia (1996) also report that the impulse may play a significant role during the formation process.

All quantities shown in figure 16(*a–f*) are normalized with the nozzle diameter ($D_{nozzle} = 0.05$ m). Part (*a*) shows the normalized position of the piston L^*_{piston} versus the normalized time t^*. From the definition given in equation (16), these two variables are equivalent. Therefore, the linear function with an exponent of one fits perfectly.

The definition of the time variable t^{**} of the abscissa for the quantities shown in figure 16(*b–f*) is different to the time variable t^* used before (equation (16)). This is explained as follows. Referring to Kaden (1931), the formation laws describe a 'self-similar enlargement of an existing flow structure'. As the acceleration is different for each of the three velocity functions, the start of the formation of a ring vortex takes place at different points in time after the beginning of the ejection. The time t^{**} primarily starts with the beginning of the formation process. As above, t^* denotes the normalized time counted from the beginning of ejection. ${t_0}^*$ denotes the normalized physical time when a vortex structure can be detected. Thus, t^{**} denotes the relative time with respect to the time at which the formation process starts:

$$t^{**} = t^* - t_0^* = \frac{L_{piston}(t) - L_{piston}(t_0)}{D_{nozzle}}. \tag{18}$$

The stronger the acceleration of the piston, the earlier the formation process begins. As above, the time t^{**} is expressed as a 'dimensionless distance'. In contrast to the case where the piston velocity is constant, the dependence between dimensionless time and dimensionless distance is nonlinear. For clarity and for the comparison with the scaling laws it will furthermore be called a 'dimensionless time'. The reason, why it is necessary to use definition (18) is the following. If using a piston velocity, which changes in time, the process of formation and also the shape of the vortex depends on the amount of fluid ejected and not on the physical time. Therefore, the position of the piston is the dominating relevant parameter. Using the time-dependent functions for the piston velocity the physical time is 'stretched' and 'compressed' compared to the process with a constant piston velocity, which was examined in § 3.2.1.

Figure 16(*b*) shows the normalized distance between the actual axial position of the jet front and the axial position of the front at the beginning of vortex formation $(X_F - X_{F,0})^*$. The calculated data matches perfectly with a linear function with exponent 0.95. Nitsche (2001) found a linear dependence with an exponent of one for the axial position of the jet front.

The curve of the normalized radial coordinate of vortex centre R^*_V (figure 16*c*) and the curve of the normalized diameter of the vortex spiral D^*_S (figure 16*d*) is almost the same for all velocity functions. Both quantities exhibit a time dependence which is proportional to $(t^{**})^{2/3}$.

In contrast, the curve of the normalized axial coordinate X^*_V (figure 16*e*) is proportional to $(t^{**})^{3/2}$ for all velocity functions considered. This behaviour is the same as given by the calculations and measurements of the experiments performed by Didden (1979) (see § 3.2.1). Didden (1979) explained the difference between the power (2/3 in the similarity law and 3/2 in the measurements) by the enlargement of

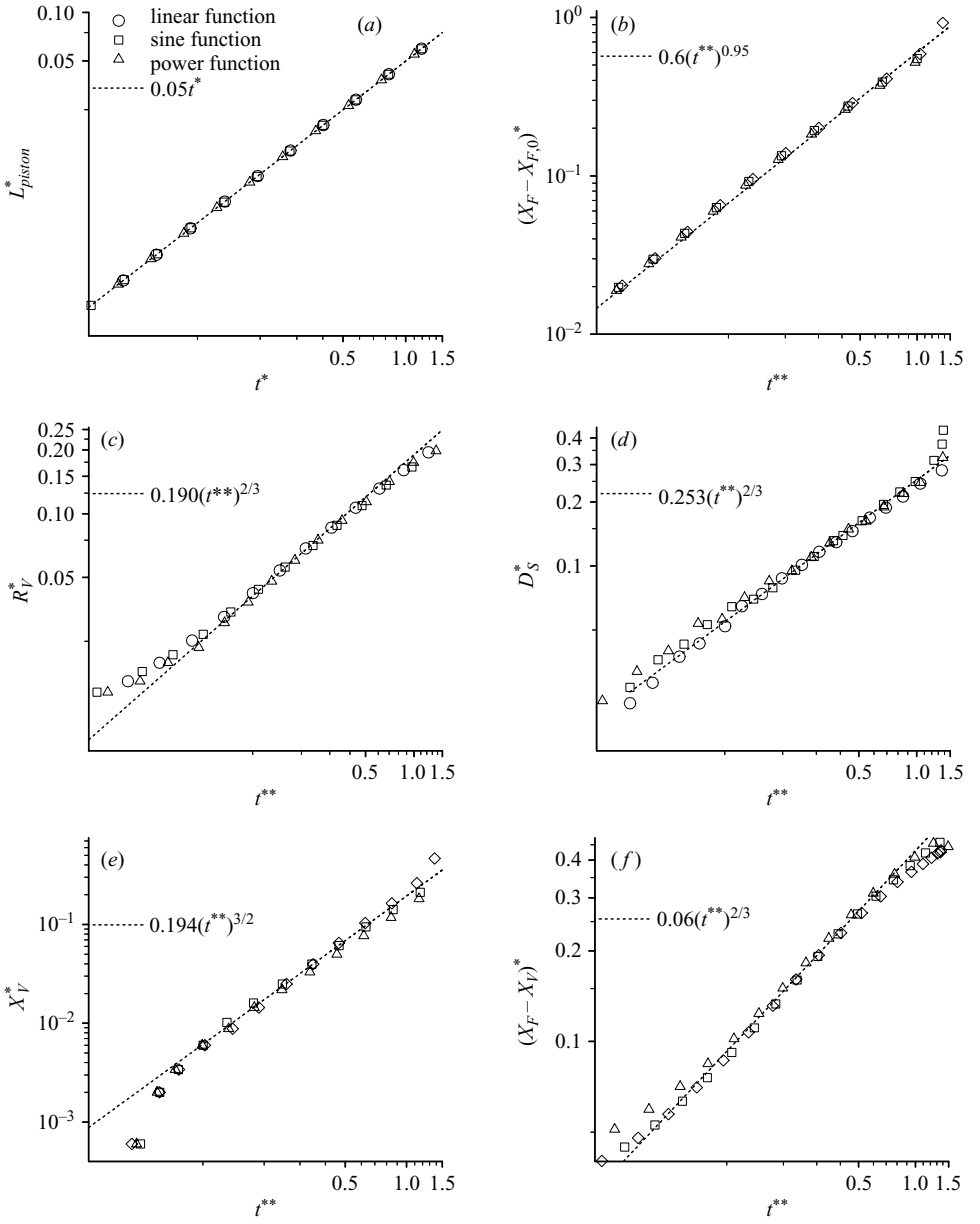

FIGURE 16. Calculations with variation of piston velocity function; (*a*) normalized position of piston L^*_{piston}; (*b*) normalized distance between axial positions of actual front and front at the beginning of vortex formation $(X_F - X_{F,0})^*$; (*c*) normalized radial position of vortex R^*_V; (*d*) normalized diameter of vortex spiral D^*_S; (*e*) normalized axial position of vortex X^*_V; (*f*) normalized distance between axial positions of jet front and vortex centre $(X_F - X_V)^*$.

the translational velocity U_V of the vortex centre due to the curvature of the vortex tube. In the following we show that the difference arises due to the use of different coordinate systems in both flow systems.

The analytical investigations of the formation of plane vortices, developing from the roll-up of a discontinuity plane and leading to the similarity laws (Kaden 1931)

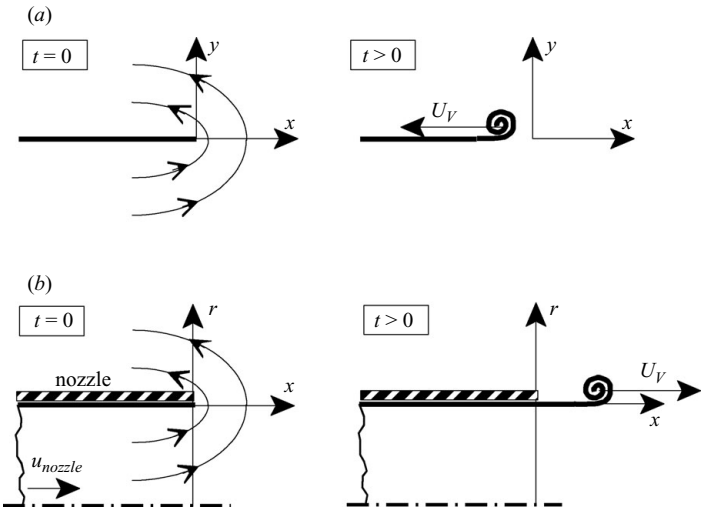

FIGURE 17. (*a*) Roll-up of a semi-infinite plane discontinuity sheet (see Kaden 1931); (*b*) roll-up of a circular vortex sheet downstream of a nozzle edge.

and the formation process which takes place downstream of a circular nozzle (Didden 1979 and this work) exhibit a translational velocity U_V of different signs (figure 17). The plane vortex investigated by Kaden (1931) moves in the negative x-direction. For the formation downstream of the nozzle edge the vortex moves inside a velocity field, which is influenced by the nozzle flow. During the formation process the vortex therefore moves in the positive x-direction. This was also discovered by Nitsche (1996). Consequently, this finding was considered during the analysis of the results of our calculations.

As shown in § 2.1.4 an axial position of the jet front X_F can be defined. The fluid which is driven radially outwards from the jet and entrained into the vortex has an axial velocity. Therefore, the movement of X_F in time can be considered as an additional velocity which is superimposed to the movement of the vortex which originates from the roll-up process. As can be seen in figure 4, the distance between the front position X_F and the vortex centre X_V increases over time during the formation process. With respect to the front position X_F the vortex moves in the negative x-direction. Now, the sign of the velocity U_V is the same as in the case considered by Kaden (1931). This relative distance normalized with the nozzle diameter $(X_F - X_V)^*$ is shown in figure 16(f). As can be seen, the relative position exhibits a time dependence which is predicted by the similarity law $(t^{**})^{2/3}$.

For the conditions used in this work, the formation laws derived for plane inviscid vortices are found to be valid also for the formation of viscous ring vortices. Inversely, it can be stated that the curvature of the vortex tube has a negligible influence on the formation process of the ring vortex.

The correspondence of the results of the calculations and the similarity laws additionally verifies that the definition of the 'dimensionless time' t^{**}, given above, is the appropriate parameter to express the progress of vortex formation. Accurately described, the 'dimensionless time' is a 'dimensionless position'. This shows that the position of the piston and not the physical time is the relevant parameter for describing the vortex formation using the time-dependent velocity of the piston.

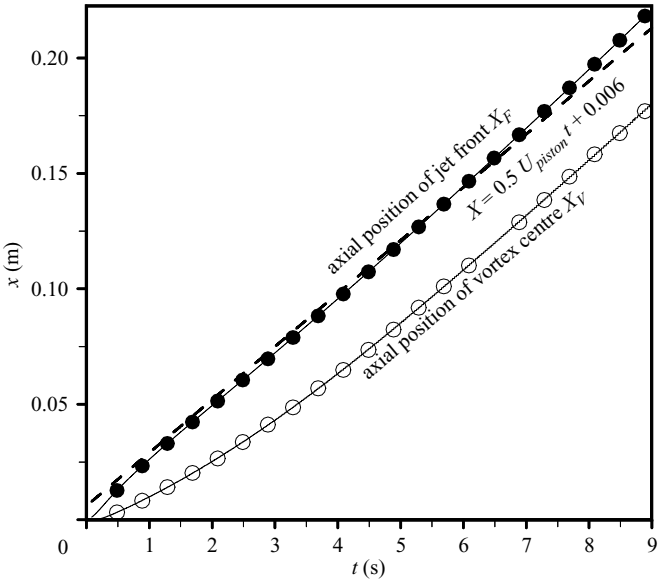

FIGURE 18. Axial positions of jet front and vortex centre versus time.

3.2.3. *Calculations with a permanent velocity*

The start-up procedure of a laminar jet described in § 2.1.4 was investigated numerically using the system described in § 3.1.1 (figure 7). In this case, the velocity at the inlet boundary was set to $U_{piston} = 0.046\,\mathrm{m\,s^{-1}}$ and held constant in time. The calculation was performed up to a physical time of 9 s.

In figure 18 the motion of distinct axial positions over time is shown. It can be seen that the axial position of the jet front X_F reaches a constant velocity of half of the nozzle exit velocity after approximately 1 s. This verifies the theory, which predicts a factor of 0.5 (see § 2.1.4). The change of the axial position of the vortex centre X_V shows a distinct acceleration phase. After a time of approximately 4 s, a translational velocity is reached which is nearly the same as the velocity U_F of the jet front. The vortex is quasi-fixed to the jet front and moves downstream with it.

As can be seen in figure 19, both the radial position of the vortex centre R_V and the diameter of the vortex spiral D_S increase with time. This is because the volume V_V of the vortex increases.

Starting from equation (6) we can derive more dependences. As the jet front moves with half of the velocity of the outflow, the volume flux of fluid emanating from the jet and flowing radially outwards into the vortex $\dot{V}_{V,\,from\,jet}$ is half of the volume flux through the nozzle:

$$\dot{V}_{V,\,from\,jet} = \frac{1}{2}\dot{V}_{nozzle} = \frac{1}{2}U_{piston}\pi\frac{{D_{nozzle}}^2}{4} = 4.52\times10^{-5}\,\mathrm{m^3\,s^{-1}}. \tag{19}$$

During the roll-up process, the vortex entrains ambient fluid into the spiral structure (see figure 9). An analysis of the vortex structure for late time justifies the assumption that the volume flux of fluid entrainment is small. Let us further assume that the vortex has a perfect toroidal geometry inside the region which is defined by the diameter of the vortex spiral D_S. The volume of a torus is defined by $V = (\pi^2/2)D_S^2 R_V$. Thus, the

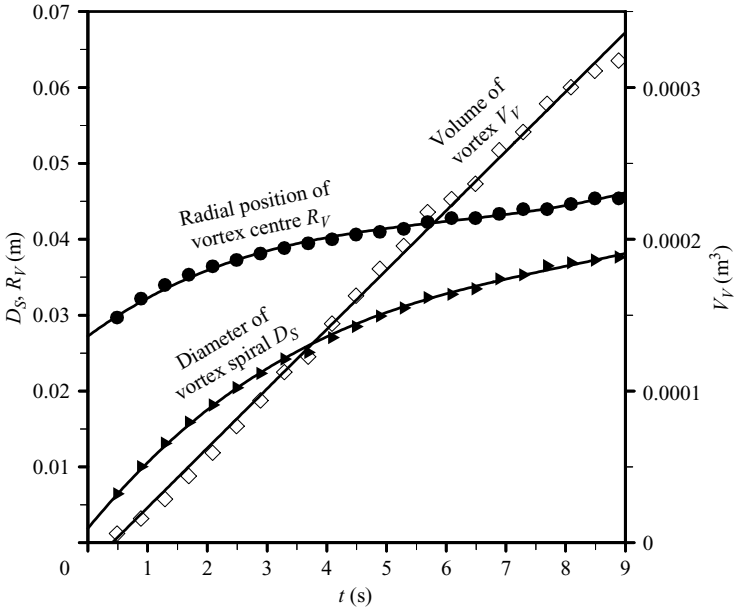

FIGURE 19. Radial position of vortex centre, diameter of spiral and volume of vortex (equation (20)) versus time.

time-dependent volume of the vortex can be expressed as

$$V_V(t) = \frac{\pi^2}{2} D_S^2(t) R_V(t), \tag{20}$$

and should be proportional to the time t. $V_V(t)$ is plotted in figure 19 (square symbols). The result shows that our assumptions are confirmed very well by the calculation. The volume of the vortex V_V, calculated by equation (20), increases linearly in time.

4. Summary

Analytical investigations by several authors (Kaden 1931; Anton 1939; Wedemeyer 1961; Pullin 1978) show that there are similarity laws for the roll-up process of inviscid plane vortex sheets. These laws describe the time-dependent axial and lateral position X_V and Y_V of the vortex centre, respectively, as well as the diameter of the vortex spiral D_S. The main goal of this work was to clarify how far these similarity or scaling laws are valid for the formation of free viscid vortex rings.

The formation process of laminar vortex rings has been investigated numerically using a CFD (computational-fluid-dynamics) code. The calculations were based on a geometry which was investigated experimentally by Didden (1979). Thereby, laminar ring vortices are generated by ejecting an amount of water using a piston from a circular nozzle into a quiescent environment.

A comparison between calculated and measured data shows a very good agreement for the time-dependent axial and radial positions (X_V, R_V) of the vortex centre as well as the velocity field at the nozzle outlet plane. The calculated and measured data differ with respect to the diameter D_S of the vortex spiral. It was shown that the difference must originate from a different definition of the spiral diameter in the experiment and in the calculations. The definition of the diameter used in the

calculations is the same as used in the derivation of the similarity laws. This can be seen in the correspondence of the time dependence of the calculated diameter D_S and the associated similarity law.

Further calculations were made, forcing the velocity of the piston by three different time-dependent functions. The results of the calculations show that the formation laws for plane vortices are also valid for the normalized axial and radial position X_V^* and R_V^*, respectively, as well as for the normalized diameter of the vortex spiral D_S^* of ring vortices. These dependences can be written as (Saffman 1978)

$$X_V^* \sim (t^{**})^{2/3}, \quad R_V^* \sim (t^{**})^{2/3}, \quad D_s^* \sim (t^{**})^{2/3}.$$

Furthermore, it was found that the similarity laws are valid only if the starting time of the formation process with respect to the starting time of the ejection is taken into account, leading to the normalized time t^{**}. More accurately, this dimensionless time is a dimensionless distance, because for a non-constant piston velocity the position of the piston is the relevant parameter, not the physical time. Consequently, the process has to be considered in a special frame of reference which moves with the front of the jet.

Additionally, the start-up process of a free jet flow was calculated. It is known from analytical considerations that the front of the jet moves with half of the velocity of the nozzle outflow. The results of the calculations confirm this dependence. After a phase of acceleration, the vortex moves downstream with the same velocity as the jet front. The time-dependent volume of the vortex spiral is proportional to the time t and can be expressed as

$$V_V(t) = \frac{\pi^2}{2} D_S^2(t) R_V(t).$$

This work was founded by the DFG (Deutsche Forschungsgemeinschaft) under project number BO693/12-1. The support is gratefully acknowledged.

REFERENCES

Anton, L. 1939 Ausbildung eines Wirbelpaares an den Kanten einer Platte. *Ing. Arch.* **10**, 411–427. (English trans. *NACA Tech. Memo.* 1398 (1956)).

Auerbach, D. 1987 Experiments on the trajectory and circulation of the starting vortex. *J. Fluid Mech.* **183**, 185–198.

Brady, M., Leonard, A. & Pullin, D. I. 1998 Regularized vortex sheet evolution in three dimensions. *J. Comput. Phys.* **146**, 520–545.

Chorin, A. J., & Bernard, P. S. 1973 Discretization of a vortex sheet, with an example of Roll-up. *J. Comput. Phys.* **13**, 423–429.

Didden, N. 1977 Untersuchung laminarer, instabiler Ringwirbel mittels Laser-Doppler-Anemometrie. *Mitteilungen aus dem Max-Planck-Institut für Strömungsforschung und der Aerodynamischen Versuchsanstalt, Herausgegeben von E.-A. Müller und H. Schlichting, Göttingen.*

Didden, N. 1979 On the formation of vortex rings: rolling-up and production of circulation. *Z. Angew. Math. Phys.* **30**, 101–116.

Durst, F. & Fuchs, W. 1974 Die Bildung von Wirbelringen durch fallende Tropfen und die Dynamik der Wirbelringfortbewegung. *Bericht* SFB 80/ET/23, Sonderforschungsbereich 80, Ausbreitungs- und Transportvorgänge in Strömungen, Universität Karlsruhe (TH).

Fabris, D. & Liepmann, D. 1997 Vortex ring structure at late stages of formation. *Phys. Fluids* **9**, 2801–2803.

Glezer, A. 1988 The formation of vortex rings. *Phys. Fluids* **31**, 3532.

Gosman, A. D. & Ideriah, F. J. K. 1976 TEACH-2E: A general computer program for two-dimensional, turbulent, recirculating flows. *Report*, Department of Mechanical Engineering, Imperial College, London.

Gühler, M. & Sallet, D. W. 1979 The formation of vortex rings and their initial motion. *Z. Flugwiss. Weltraumforsch.* **3**, 109–155.

Heeg, R. S. & Riley, N. 1997 Simulations of the formation of an axisymmetric vortex ring. *J. Fluid Mech.* **339**, 199–211.

Hettel, M. 2006 Analytische und numerische Untersuchungen der Dynamik von Vormischflammen sowie deren Interaktion mit Ringwirbelstrukturen. PhD thesis, University of Karlsruhe.

Hettel, M., Büchner, H., Habisreuther, P., Bockhorn, H. & Zarzalis, N. 2004 Modeling of ring-vortices and their interaction with turbulent premixed flames. *Combust. Sci. Tech.* **176**, 835–850.

Hettel, M., Büchner, W., Weib, H., Habisreuther, P., Bockhorn, H. & Zarzalis, N. 2005 URANS - Modelling of pulsed turbulent jets and premixed jet flames. *Prog. Comput. Fluid Dyn.* **5**, 386–397.

Hirsch, C. 1995 Ein Beitrag zur Wechselwirkung von Turbulenz und Drall. PhD thesis, University of Karlsruhe.

James, S. & Madnia, C. K. 1996 Direct numerical simulation of a laminar vortex ring. *Phys. Fluids* **8**, 2400–2414.

Kaden, H. 1931 Aufwicklung einer unstabilen Unstetigkeitsfläche. *Ing. Arch.* **2**, 140–169. (English trans. R. A. Lib. Trans. no. 403).

Leonard, A. 1980 Vortex methods for flow simulation. *J. Comput. Phys.* **37**, 289–335.

Liess, C. 1978 Experimentelle Untersuchung des Lebenslaufes von Ringwirbeln. *Max-Planck-Institut für Strömungsforschung, Göttingen, Bericht* 1/1978.

Liess, C. & Didden, N. 1976 Experimente zum Einfluß der Anfangsbedingungen auf die Instabilität von Ringwirbeln. *Z. Angew. Math. Mech.* **56**, 206–208.

Lugt, H., J. 1983 *Vortex flow in Nature and Technology*, John Wiley & Sons. (Translation of: *Wirbelströmungen in Natur und Technik*, G. Braun.)

Maxworthy, T. 1972 The structure and stability of vortex rings. *J. Fluid Mech.* **51**, 15–32.

Maxworthy, T. 1976 Some experimental studies of vortex rings. *J. Fluid Mech.* **81**, 465–495.

Mohseni, K., Ran, H. & Colonius, T. 2001 Numerical experiments on vortex ring formation. *J. Fluid Mech.* 430, 267–282.

Moore, D. W. 1974 A numerical study of the roll-up of a finite vortex sheet. *J. Fluid Mech.* **63**, 225–235.

Nitsche, M. 1996 Scaling properties of vortex ring formation. *Phys. Fluids* **8**, 1848–1855.

Nitsche, M. 2001 Self-similar shedding of vortex rings. *J. Fluid Mech.* **435**, 397–407.

Nitsche, M. & Krasny, R. 1994 A numerical study of vortex ring formation at the edge of a circular tube. *J. Fluid Mech.* **276**, 139–161.

Noll, B. 1992 Evaluation of a bounded high resolution scheme for combustor flow computations. *AIAA J.* **30**, (1).

Patankar, S. V. 1980 *Numerical Heat Transfer and Fluid Flow*. Hemisphere.

Prandtl, L. 1924 Über die Entstehung von Wirbeln in der idealen Flüssigkeit, mit Anwendung auf die Tragflügeltheorie und andere Aufgaben. *Vorträge aus dem Gebiet der Hydro- und Aerodynamik, Herausgegeben v. Th. v. Kármán u. T. Levi-Civita.* 19–34, Berlin.

Pullin, D. I. 1978 The large-scale structure of unsteady self-similar rolled-up vortex sheets. *J. Fluid Mech.* **88**, 401–430.

Rosenfeld, M., Rambod, E. & Gharib, M. 1998 Circulation and formation number of laminar vortex rings. *J. Fluid Mech* **376**, 292–318.

Saffman, P. G. 1978 The number of waves on unstable vortex rings. *J. Fluid Mech.* **84**, 625–639.

Saffman, P. G. 1992 *Vortex Dynamics.* Cambridge University Press.

Sallet, D. W. & Widmayer, R. S. 1974 An experimental Investigation of laminar and turbulent vortex rings in air. *Z. Flugwiss.* **22**, 201–215.

Schneider, E. 1978 Werden, Bestehen, Instabilität, Regeneration, Vergehen eines Ringwirbels. *Max-Planck-Institut für Strömungsforschung, Göttingen, Bericht* 17/1978.

Schneider, E. 1980 Experimentelle Untersuchung der Instabilitätsphasen eines laminaren Ringwirbels im Hinblick auf vergleichbare Instabilitätsereignisse in turbulenten Scherschicht-, Grenzschicht- und Kanalströmungen. *Max-Planck-Institut für Strömungsforschung, Göttingen, Bericht* 17/1980.

Seno, T., Kageyama, S. & Ito, R. 1988 A modeling of vortex rings in an axisymmetric pulsed jet. *J. Chem. Engng Japan* **21**, 1–5.

Shariff, K. & Leonard, A. 1992 Vortex rings. *Annu. Rev. Fluid. Mech.* **24**, 235.

Southerland, K. B., Porter, J, R., Dahm, W. J. A. & Buch, K. A. 1991 An experimental study of the molecular mixing process in an axisymmetric laminar vortex ring. *Phys. Fluids* A **3**, 1385–1392.

Wedemeyer, E. 1961 Ausbildung eines Wirbelpaares an den Kanten einer Platte. *Ing. Arch.* **30**, 187–200.

Wille, R. 1952 Über Strömungserscheinungen im Übergangsgebiet von geordneter zu ungeordneter Bewegung. *Jahrbuch der Schiffbautechnischen Gesellschaft* **46**, 176–187.